A model of selective masking in chromatic detection

Timothy G. Shepard Department of Psychology, Northeastern University, Boston, MA, USA

Emily A. Swanson Department of Psychology, Northeastern University, Boston, MA, USA

Comfrey L. McCarthy Department of Psychology, Northeastern University, Boston, MA, USA

Rhea T. Eskew, Jr. Department of Psychology, Northeastern University, Boston, MA, USA

Narrowly tuned, selective noise masking of chromatic detection has been taken as evidence for the existence of a large number of color mechanisms (i.e., higher order color mechanisms). Here we replicate earlier observations of selective masking of tests in the (L,M) plane of cone space when the noise is placed near the corners of the detection contour. We used unipolar Gaussian blob tests with three different noise color directions, and we show that there are substantial asymmetries in the detection contours—asymmetries that would have been missed with bipolar tests such as Gabor patches. We develop a new chromatic detection model, which is based on probability summation of linear cone combinations, and incorporates a linear contrast energy versus noise power relationship that predicts how the sensitivity of these mechanisms changes with noise contrast and chromaticity. With only six unipolar color mechanisms (the same number as the cardinal model), the new model accounts for the threshold contours across the different noise conditions, including the asymmetries and the selective effects of the noises. The key for producing selective noise masking in the (L,M) plane is having more than two mechanisms with opposed L- and M-cone inputs, in which case selective masking can be produced without large numbers of color mechanisms.

Introduction

By the mid-1980s, a consensus had developed on the outlines of a model of color detection and discrimination, one that seemed to explain both psychophysics and lateral geniculate nucleus physiology (Boynton, 1979; Lennie & D'Zmura, 1988). This model primarily was based on data collected by Krauskopf, Williams, and Heeley (1982), who used habituation to find the "cardinal axes" (mechanism-isolating directions) of color space. An elaborated version of a model based on this work, with the original bipolar color channels split into unipolar pairs (Eskew, 2009; Sankeralli & Mullen, 1997, 2001), is shown in Figure 1. However, the cardinal consensus was shattered by evidence, summarized in Eskew (2009), Krauskopf (1999), and Hansen and Gegenfurtner (2013), showing that this simple model is incorrect. Instead, Krauskopf, Williams, Mandler, and Brown (1986) argued that there were instead many "higher order" color mechanisms, initially conceived of as recombinations of the cardinal mechanisms, tuned to a large variety of hues.

Some of the best evidence against the cardinal axis model consists of selective masking or habituation, in which the threshold-elevating effect is tuned to very specific color directions rather than being broadly tuned, as the cardinal axis model would predict. For example, Hansen and Gegenfurtner (2013) put masking noise near the corner of the detection contour in the (L,M) plane—the plane of cone space in which the S-cones are unmodulated—and found highly selective masking. Noises near the corners produced maximum masking at those specific angles and much less even at very close angles. Their interpretation was that there are a great many higher order mechanisms.

Following Hansen and Gegenfurtner (2013), we measured detection contours in the (L,M) plane in the present study with and without masking noise; the noise was placed near the corners of the contour (where the underlying mechanisms have equal sensitivity). We

Citation: Shepard, T. G., Swanson, E. A., McCarthy, C. L., & Eskew, R. T., Jr. (2016). A model of selective masking in chromatic detection. *Journal of Vision, 16*(9):3, 1–17, doi:10.1167/16.9.3.

doi: 10.1167/16.9.3 Received January 31, 2016; published July XX, 2016 ISSN 1534-7362

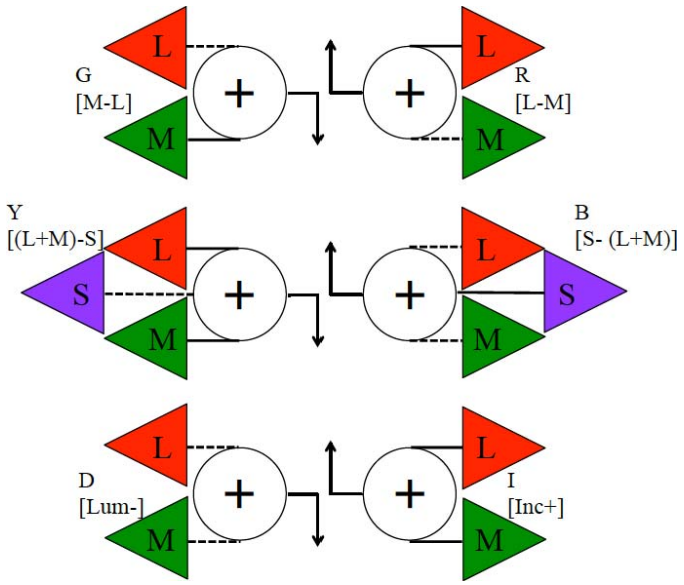

Figure 1. An extension of the cardinal model that contains three rectified symmetric pairs of mechanisms: a separate mechanism for the detection of L − M and another for the detection of M − L, separate mechanisms for S − (L + M) and (L + M) − S, and separate mechanisms for a luminance increment (I) and decrement (D). The dashed lines represent sign inversion. Modified from Eskew (2009).

replicated the main effect of Hansen and Gegenfurtner (2013) by finding that the effect of the noise was in some cases selective: The maximum threshold elevation was at or near the noise direction. However, we show that a model can produce selective masking effects with only six mechanisms—the same number as the cardinal mechanisms model. The key feature of the model that allows for selective masking in the (L,M) plane is the presence of more than two mechanisms with opposed L- and M-cone inputs.

Method

Observers

Four well-practiced observers (TGS, CLM, SAF, and NO) participated in the experiment. Authors TGS and CLM participated in all four noise conditions, observer SAF participated in three conditions, and observer NO participated in two. All had normal scores on the Farnsworth-Munsell 100-hue test (Farnsworth, 1943) and the Ishihara plates. Northeastern University's institutional review board approved the research protocol, and the procedures complied with the Declaration of Helsinki.

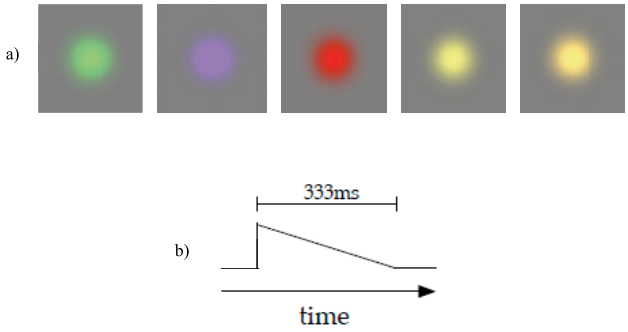

Figure 2. (a) The test stimuli were circular Gaussian blobs ($\sigma = 1°$). (b) The stimuli were presented with a rapid-start profile "sawtooth" of 333-ms total duration.

Apparatus

Stimuli were created on a Power Macintosh computer and displayed on a Sony GDM-F520 cathode ray tube monitor running at 75 Hz using an ATI Radeon 7500 video board with a driver verified to support the 10-bit digital-to-analog converters. Spectroradiometric calibration was performed at 4-nm intervals across the spectrum using a Photo Research PR-650 spectroradiometer, and the monitors were linearized with the gamma correction lookup tables. Observers were corrected to normal visual acuity using a trial lens that was placed in front of their dominant eye; the other eye was patched. Head position was stabilized with a chin and forehead rest. All experiments were conducted in a dark room.

Test and noise stimuli

The test stimuli were circular Gaussian blobs ($\sigma = 1°$) presented against a gray background field with a rapid-start "sawtooth" profile of 333-ms total duration (Figure 2). The sawtooth profile was chosen to maximize the likelihood of separating On and Off responses. Fixation was guided by four black diagonal lines pointing at the center of the screen (ending 1.5° from the center), which were present throughout the experiment.

The masking noise consisted of horizontal lines that were superimposed on the test (Figure 3). The lines randomly and independently changed from one chromaticity to a symmetrically opposite chromaticity (on the opposite side of the white point) so that the mean chromaticity was unchanged. Each line switched chromaticity with probability 1/2 at 18.75 Hz. The power spectrum of the noise is plotted in figure 2 of Wang, Richters, and Eskew (2014); it is dominated by low spatial and temporal frequencies. The noise contrast was always 90% of the maximum available at the noise direction. In cone contrast units, the noise

Figure 3. Chromatic noise. The lines randomly and independently changed from one chromaticity to a symmetrically opposite chromaticity (on the opposite side of the white point) so that the mean chromaticity was unchanged. Each line switched chromaticity with probability 1/2 at 18.75 Hz.

cone contrast vector length $|\mathbf{n}|$ (Appendix A) was 0.498, 0.414, and 0.267 for the 42°/222°, 48°/228°, and 64°/244° noises, respectively.

All of the stimuli were half toned; 2-pixel horizontal lines of noise alternated with 2-pixel lines of test (see Giulianini & Eskew, 1998). The high spatial frequency components in the test that were created by this half-toning procedure generally were not visible, except occasionally for tests with color directions near the ends of the contour in the no-noise condition. Note that the test was always half toned whether the noise was present or not, and thus the test profile was the same in all conditions. Detection thresholds were measured at many different chromatic angles in the (L,M) plane (three to five runs of 100 trials at each angle).

Procedure

Detection

A two-alternative forced-choice adaptive staircase procedure was used to measure detection thresholds. Observers adapted to the gray background field for 90 s before each run of 100 trials. In the noise conditions, the observer adapted to the gray background plus the modulating noise (when present). In each run, a single test color direction (and noise color direction in the masking conditions) was used.

Each trial consisted of two 333-ms intervals signaled by tones and separated by 400 ms. The observer was asked to determine which interval the test stimulus appeared in and received feedback after each response. The stimulus contrast was decreased by 0.1 log unit after three consecutive correct responses and increased by the same amount after one incorrect response. Weibull functions were fit to the accumulated frequency-of-seeing data for each run using a maximum likelihood method to estimate two parameters of the psychometric function: a threshold estimate (corresponding to a detection rate of 82%) and an estimate of the psychometric slope. After fitting the Weibull functions, thresholds from multiple runs were averaged (three to five runs at each color angle); standard errors were calculated using between-runs (mostly between-sessions) variances. Additional runs were added in cases where the coefficient of variation was unusually high. The data reported here represent results from more than 110,000 forced-choice trials.

Color representation

Stimuli are represented in two color spaces in this article. Because its units are nonarbitrary, cone contrast space is the primary representation used, and when angles and distances are given they refer to cone contrast space. In this space, the axes represent the modulation of the cones relative to the steady excitation produced by the mean adapting field in meaningful units. The contrast of the stimulus, $|\mathbf{t}|$, is defined as the Euclidean distance from the origin to the ($\Delta L/L$, $\Delta M/M$) point representing the peak of the stimulus:

$$|\mathbf{t}| = \sqrt{\left(\frac{\Delta L}{L}\right)^2 + \left(\frac{\Delta M}{M}\right)^2}.$$

Reported contrasts have been halved (from the nominal, peak value) to facilitate comparison with studies not using half-toned stimuli.

The second color representation used here is a variant of a cone-excitation space, here called MacLeod-Boynton-Derrington-Krauskopf-Lennie (MBDKL) space. In the (L,M) plane of this space, the horizontal axis represents the difference of the L- and M- cone excitations, and the vertical axis represents their sum; L-cone excitation increases to the right and up. This space represents changes in the cone quantal catch from the mean adaptive field in arbitrary units. Here we normalize the distance along both the horizontal and vertical axes by threshold using the averages of the two L – M (135°/315°) and two L + M (45°/225°) no-noise thresholds for a given observer.

Detection contours in the ($\Delta L/L$, $\Delta M/M$) plane typically are quasi-elliptical, with their long axis along the 45° and 225° direction (e.g., Figure 4). As pointed out by Hansen and Gegenfurtner (2013), relative to cone contrast space, the MBDKL representation expands the chromaticities near the ends of this detection contour and can make it easier to see potential selective masking effects in this region. For

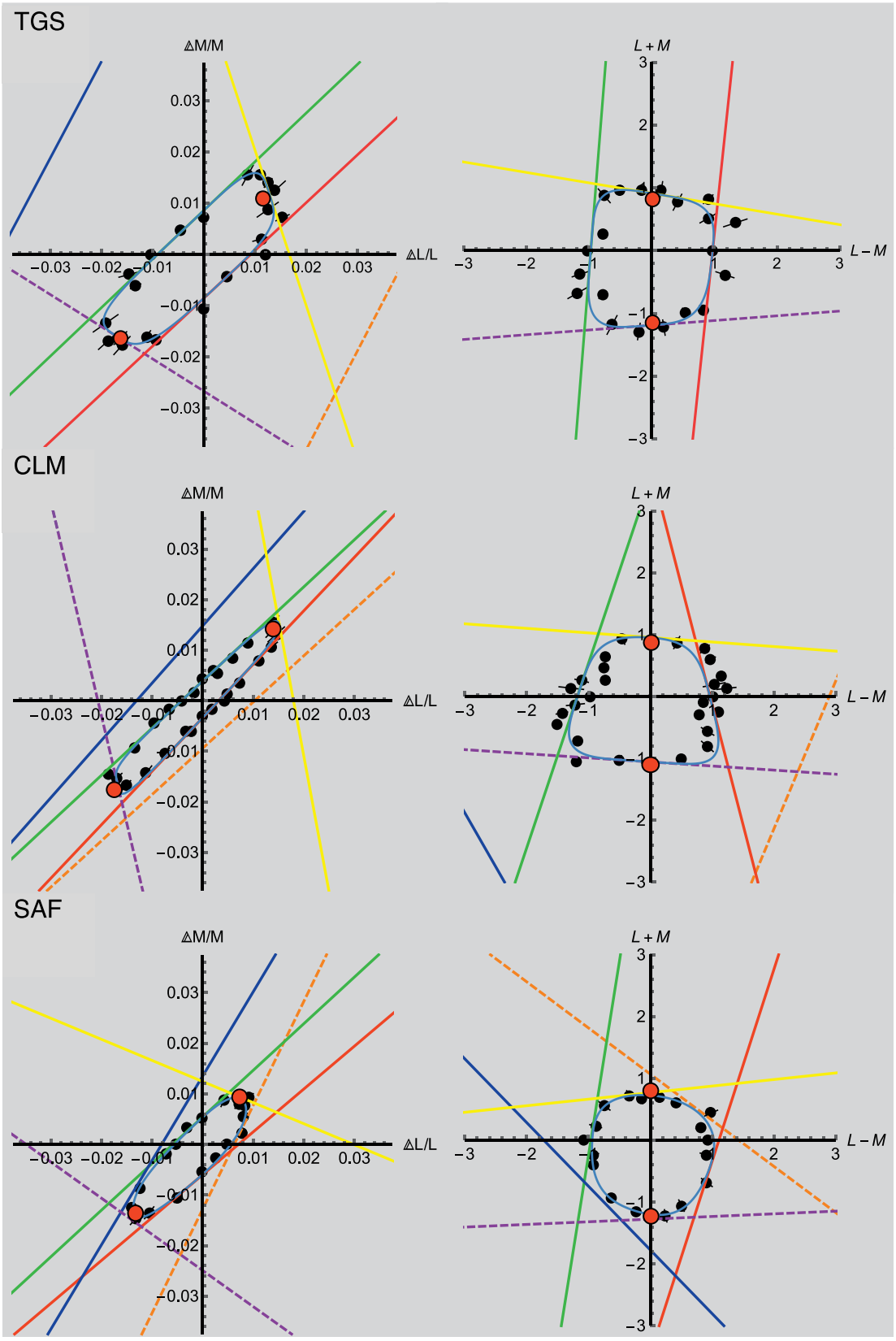

Figure 4. No-noise condition. Detection thresholds (black discs) and model fits for three observers. Colored lines represent mechanism thresholds, and the smooth closed contour is the probability sum of these mechanisms. The same data and model are represented in cone contrast space (left column) and MBDKL space (right column). The red discs denote the 45° and 225° stimulus thresholds for reference.

this reason, we show our data in both color spaces, as did Hansen and Gegenfurtner (2013).

Model

The models used in this article have, as elements, rectified linear chromatic mechanisms: weighted sums (weights W_L and W_M for the L- and M-cones, respectively), with that sum defined to be 1.0 at threshold. The mechanisms are half-wave rectified so that each mechanism responds only in one half of the chromatic space (Figure 1; Eskew, 2009). The mechanisms are combined by an approximation to probability summation, with a Minkowski exponent of 4.0. These features of the model are identical or nearly identical to those used previously by several authors (Cole, Hine, & McIlhagga, 1993; Eskew, McLellan, & Giulianini, 1999; Eskew, Newton, & Giulianini, 2001; Giulianini & Eskew, 1998; Newton & Eskew, 2003; Sankeralli & Mullen, 1996).

The novel aspect of the present model is how the mechanisms vary across noise conditions. We assume here that thresholds mediated by a single mechanism follow an energy versus noise relationship based on the theory of noise masking (Giulianini & Eskew, 2007; Wang et al., 2014), in which the contrast energy of the test is linearly related to the noise contrast power. The threshold contrast—proportional to the square root of the test contrast energy—for a test at angle τ, in the presence of the noise of contrast power $|\mathbf{n}|^2$ at angle v, is given by

$$|\mathbf{t}| = \sqrt{\frac{1}{Q_t|\mathbf{f}|^2\lfloor\cos(\alpha-\tau)\rfloor^2} + b\frac{Q_n}{Q_t}\frac{|\mathbf{n}|^2\lfloor\cos(\alpha-v)\rfloor^2}{\lfloor\cos(\alpha-\tau)\rfloor^2}} \quad (1)$$

(derived in Appendix A). The half brackets ($\lfloor\ \rfloor$) represent half-wave rectification (i.e., values less than zero are set to zero). The vector of cone contrast weights (the "mechanism vector"; Eskew et al., 1999), is $\mathbf{f}$, which takes polar angle α in the (L,M) plane ($\alpha = 0$ is the L-cone increment direction). The subscripted Qs are calculated constants that represent the energy and power in test (t) and noise (n), respectively, and the fitted parameter b represents the sensitivity of the mechanism to the spatiotemporal characteristics of the noise. The first term in the radical represents the baseline condition in which no noise was added, and the second term raises the threshold due to the noise.

The thresholds for all the tests for a given mechanism and noise condition are then combined by probability summation to account for the set of thresholds in that condition. The three free parameters for each mechanism are the two cone contrast weight components of $\mathbf{f}$ (or, equivalently, the magnitude $|\mathbf{f}|$ and its angle α) and the noise sensitivity parameter b. Below, we report the polar angle of the mechanism vector and vector length in the (ΔL/L, ΔM/M) plane (see Table 1), with asymptotic standard error estimates from the fits (and after applying the appropriate propagation of error formulae in converting from the cone weights to angles and vector lengths). The degrees of freedom for fitting the model is the number of thresholds across all noise conditions (e.g., 92 for observer TGS) minus three times the number of mechanisms (e.g., 74 degrees of freedom for observer TGS's six-mechanism model).

Equation 1 tightly constrains the model. Each mechanism must have the same polar angle in the no-noise condition and all the noise conditions, and thus its threshold loci are lines of the same slope in every condition; those lines are orthogonal to the mechanism vector $\mathbf{f}$. Even more important, for every test angle, the masking effect of the noise on the mechanism must be proportional to $\cos^2(\alpha - v)$, with the constant of proportionality bQ_n/Q_t the same for all test and noise angles detected by that mechanism. These model features are derived from theory and are consistent with prior results in both luminance and chromatic detection (Gegenfurtner & Kiper, 1992; Giulianini & Eskew, 1998; Legge, Kersten, & Burgess, 1987; Pelli, 1981; Wang et al., 2014), and collectively they make model comparisons much more powerful. For example, comparing models with different numbers of these mechanisms is not based on curve fitting but rather is a comparison of theoretical accounts of the data.

Results and discussion

No-noise condition

Figure 4 shows the thresholds for Gaussian blobs without noise for three observers (TGS, CLM, and SAF). Observer NO, who participated in only two conditions, is not shown; her limited results are consistent with those of the other observers. The points denote measured thresholds, and the small black lines through those points indicate ± 1 *SE* (based on between-sessions variability only); in many cases the error bars are smaller than the symbols. Colored lines on the plots represent mechanism thresholds (discussed below), and the smooth closed contour is the probability sum of those mechanisms. The line color is a rough indication of the hue of stimuli that lie on that line according to informal observations of the observers. For example, stimuli on or near the orange line appear "orangey red," and stimuli on or near the blue line appear "bluish."

The long flanks that comprise the majority of the measured thresholds lie near two parallel lines with the

Mechanism	Log_{10} b	Mechanism angle α (°)	Mechanism vector length	Line color
TGS ($R^2 = 0.99$)				
R	1.35 (0.13)	313 (2.9)	510.0 (26.2)	Red
G	1.39 (−0.95)	134 (2.5)	510.0 (22.6)	Green
O	1.10 (−1.04)	333 (5.6)	90.3 (8.5)	Orange
B	0.50 (−0.76)	152 (5.2)	90.2 (7.9)	Blue
Y	1.57 (−0.44)	18 (8.6)	200.9 (14.2)	Yellow
P	1.26 (−0.98)	238 (9.6)	141.21(23.9)	Purple
CLM ($R^2 = 0.99$)				
R	1.87 (0.71)	317 (2.9)	1373.8 (70.1)	Red
G	1.71 (0.25)	133 (2.9)	1123.1 (57.8)	Green
O	1.04 (−1.30)	312 (5.4)	458.7(43.2)	Orange
B	1.38 (−0.83)	139 (3.9)	325.6 (22.3)	Blue
Y	1.56 (−1.41)	11 (0.6)	180.3 (10.5)	Yellow
P	1.36 (−1.27)	193 (0.5)	158.1 (6.2)	Purple
SAF ($R^2 = 0.99$)				
R	1.33 (−0.61)	310 (0.7)	694.8 (8.1)	Red
G	2.11 (−0.95)	133 (1.5)	799.8 (20.7)	Green
O	6.94 (11.10)	334 (3.3)	567.3 (31.4)	Orange
B	2.19 (−0.76)	149 (0.6)	459.7 (5.1)	Blue
Y	1.53 (−0.44)	67 (6.6)	277.8 (27.7)	Yellow
P	1.28 (−0.98)	234 (5.9)	157.1 (15.2)	Purple

Table 1. Best-fitting parameter values for the six-mechanism model (with standard errors) for observers TGS, CLM, and SAF. Line color is the color of the mechanism threshold line in the detection contour plots.

approximate slope of +1 for all four observers. These data are qualitatively similar to many previous studies (Cole et al., 1993; Cole, Stromeyer, & Kronauer, 1990; Giulianini & Eskew, 1998) showing approximate symmetry about the main diagonal (45°/225°) and very high sensitivity of the thresholds along those long flanks (Chaparro, Stromeyer, Huang, Kronauer, & Eskew, 1993). However, there are individual differences between observers. CLM's contour is narrower than TGS's and SAF's. The aspect ratio of CLM's contour (the average of thresholds at 45° and 225° divided by the thresholds at 135°/315°) is 9.32, whereas that of TGS's is only 3.02, SAF's is 3.88, and NO's is 3.93. Compared with some previous studies (Cole et al., 1993; Sankeralli & Mullen, 1996), TGS, SAF, and NO are relatively insensitive along the flanks (for review see Eskew et al., 1999). In addition, the sets of threshold along the flanking regions converge in the first quadrant (QI), especially for CLM—an effect never observed previously—resulting in a trapezoidal detection contour when plotted in MBDKL.

There are differences between the increment and decrement thresholds at the ends of the contour. For all four observers, increment sensitivity is higher than decrement sensitivity (red points): The decrement thresholds at 225° are between 1.25- and 1.9-fold higher than the increment thresholds at 45°. A similar asymmetry has been observed previously (e.g., see figure 3b in Giulianini & Eskew, 1998).

Selective masking in the presence of chromatic noise

Thresholds in the presence of 42°/222° noise are shown in Figure 5, of 48°/228° noise are shown in Figure 6, and of 64°/244° noise are shown in Figure 7. (Note the change of scale compared with Figure 4; thresholds are anywhere from five to 20 times higher when these noises are added.) The detection contours are highly elongated in quadrants I and III (QI and QIII), as observed previously with 45° noise (Hansen & Gegenfurtner, 2013).

More important, as shown by Hansen and Gegenfurtner (2013), the masking effect of the noise is selective. Figure 8 shows threshold elevations (relative to the no-noise fitted contour) as a function of angular deviation between the test and noise angles. For the 42°/222° and 48°/228° noise conditions, threshold elevations are highest when the test angles are located very near the direction of the noise and fall steeply for tests that are only a few degrees away.

Figure 7 shows the 64°/244° noise condition for observers TGS, CLM, and SAF. The contours are substantially broader than those in Figures 5 and 6, suggesting a transition as the noise vector rotates toward the second and fourth quadrants (QII/QIV), toward the broad, nonselective noise effects observed in many previous studies with noises in QII/QIV (Eskew et al., 2001; Giulianini & Eskew, 1998). Figure 8 (red symbols) shows the less-selective effect of this noise:

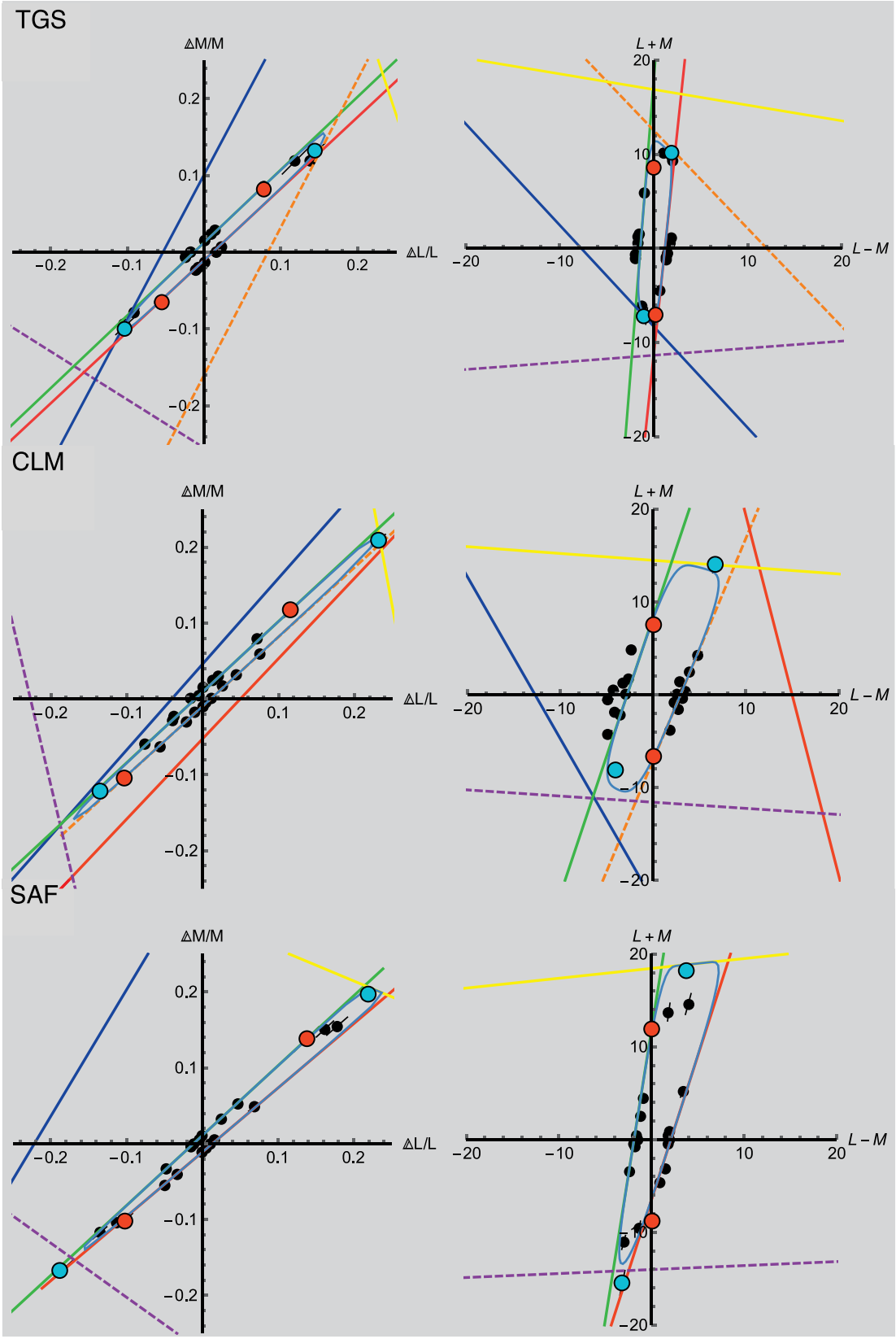

Figure 5. 42°/222° noise condition. Detection thresholds (black discs) and model fits for three observers. Colored lines represent mechanism thresholds, and the smooth closed contour is the probability sum of these mechanisms. The same data and model are represented in cone contrast space (left column) and MBDKL space (right column). The red discs denote the 45° and 225° stimulus thresholds, and the cyan discs indicate the 42° and 222° stimulus thresholds and the noise direction. Notice the scale change compared with Figure 4: Cone contrast thresholds are larger (fivefold to 20-fold) when noise is added.

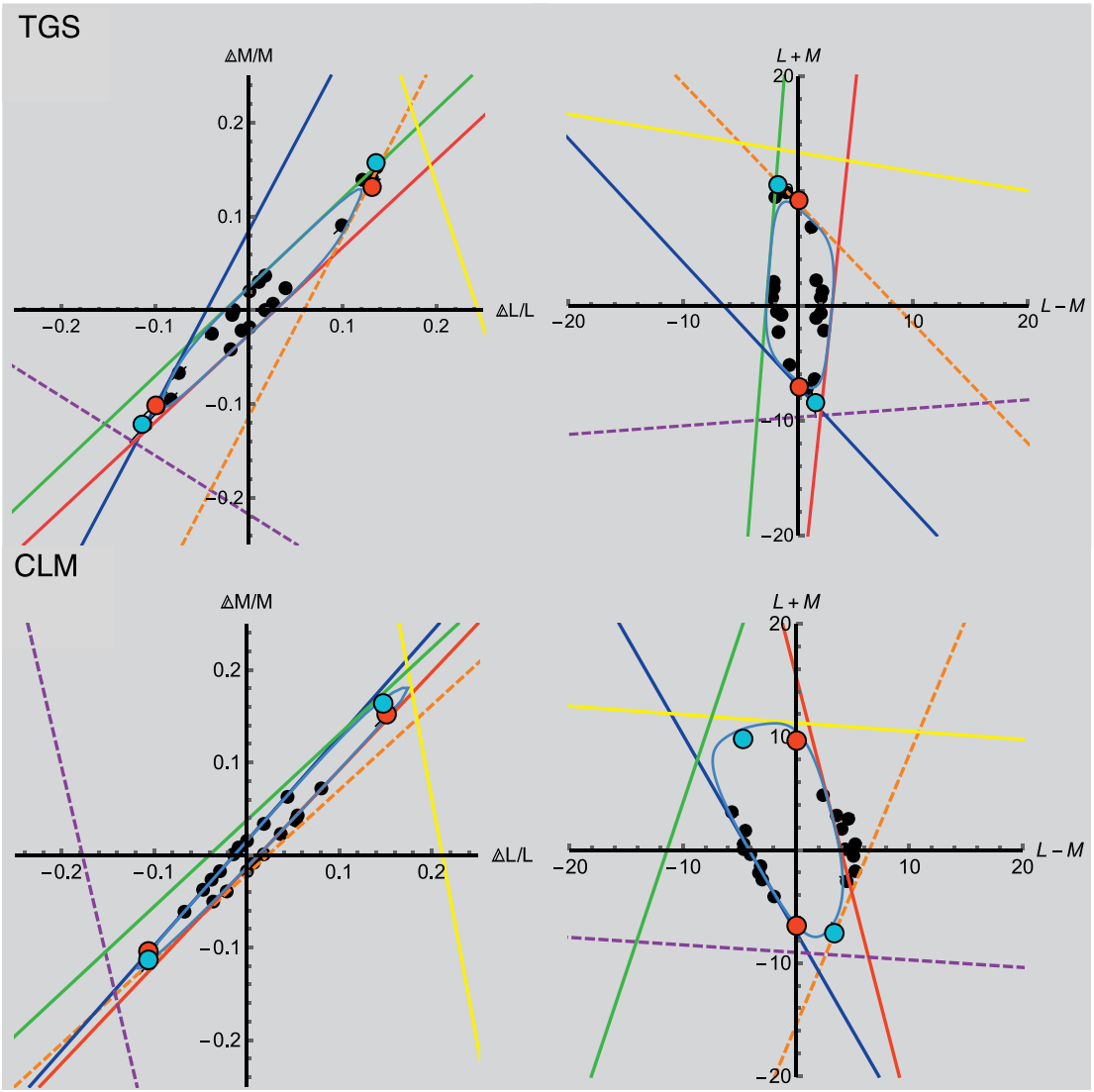

Figure 6. 48°/228° noise condition. Detection thresholds (black discs) and model fits for two observers. Colored lines represent mechanism thresholds, and the smooth closed contour is the probability sum of these mechanisms. The same data and model are represented in cone contrast space (left column) and MBDKL space (right column). The red discs denote the 45° and 225° stimulus thresholds, and the cyan discs indicate the 48° and 228° stimulus thresholds and the noise direction.

There is relatively more elevation at test angles that are further removed from the noise.

In all of the noise conditions, there are also asymmetries between increment and decrement thresholds. These asymmetries are of the opposite direction to those found in the no-noise condition (cf. Vingrys & Mahon, 1998): Thresholds near the upper end of the noise contour in QI (increments) are 1.2 to 1.5 times larger than the QIII thresholds (decrements) in all of the noise conditions. Figure 8 shows the asymmetry in terms of elevation: The peak on the left is higher than the peak on the right. This result—more masking of increments than decrements—is in the same direction as the S-cone masking studied by Wang et al. (2014). The asymmetries may be partially due to the sawtooth temporal profile of the tests, which may help separate responses from On and Off pathways (Wang et al., 2014).

Six-mechanism model

Consistent with previous findings (Eskew et al., 2001; Giulianini & Eskew, 1998), only four linear mechanisms suffice to provide an excellent fit to the thresholds in all noise conditions when each observer and noise condition is considered separately (fits not shown). In particular, in the no-noise condition for observers TGS and CLM, the set of mechanisms (red [R], green [G], yellow [Y], and purple [P]) is almost identical to mechanisms found previously (e.g., Giulianini & Eskew, 1998). Observer SAF has a small

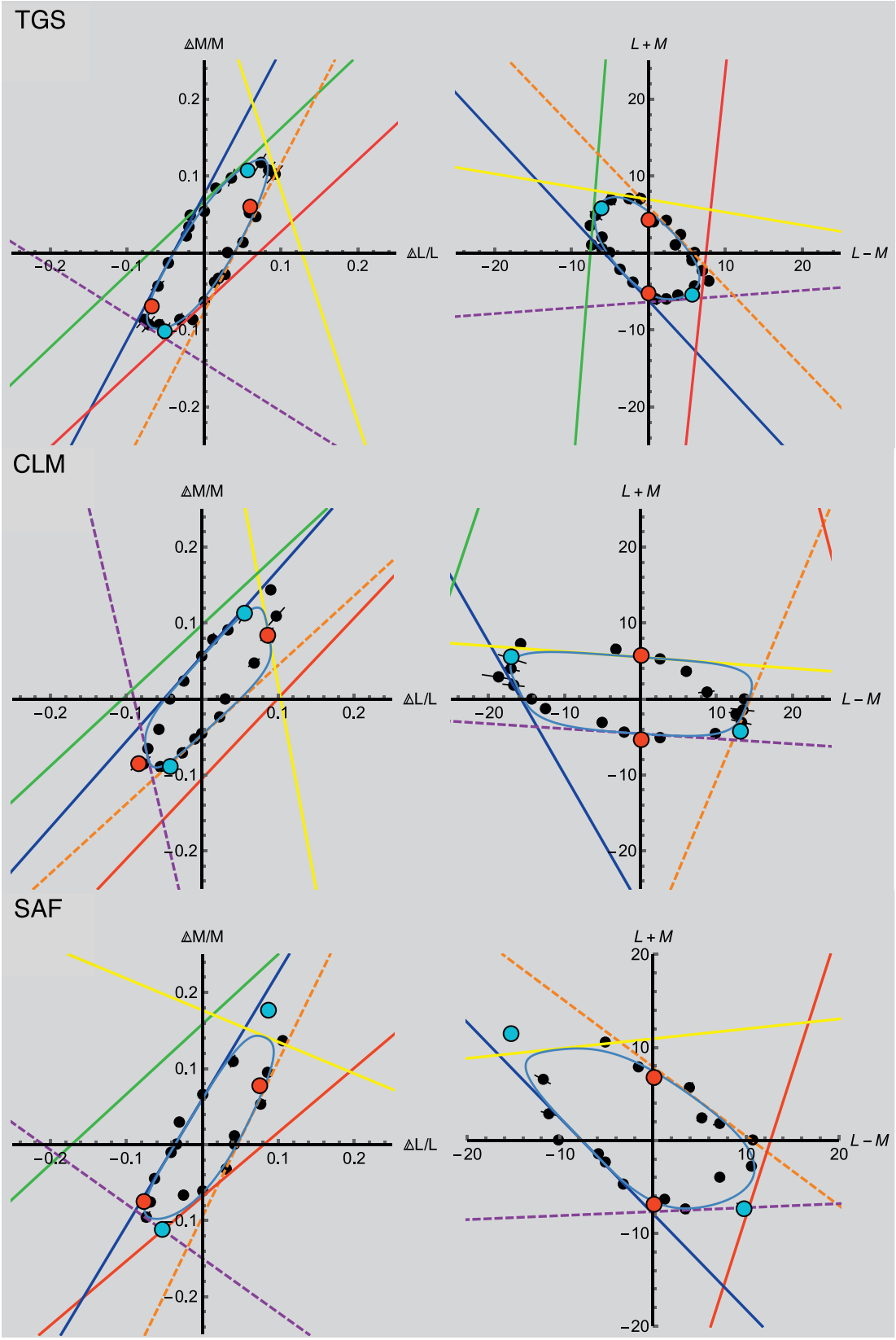

Figure 7. 64°/244° noise condition. Detection thresholds (black discs) and model fits for three observers. Colored lines represent mechanism thresholds, and the smooth closed contour is the probability sum of these mechanisms. The same data and model are represented in cone contrast space (left column) and MBDKL space (right column). The red discs denote the 45° and 225° stimulus thresholds, and the cyan discs indicate the 64° and 244° stimulus thresholds and the noise direction.

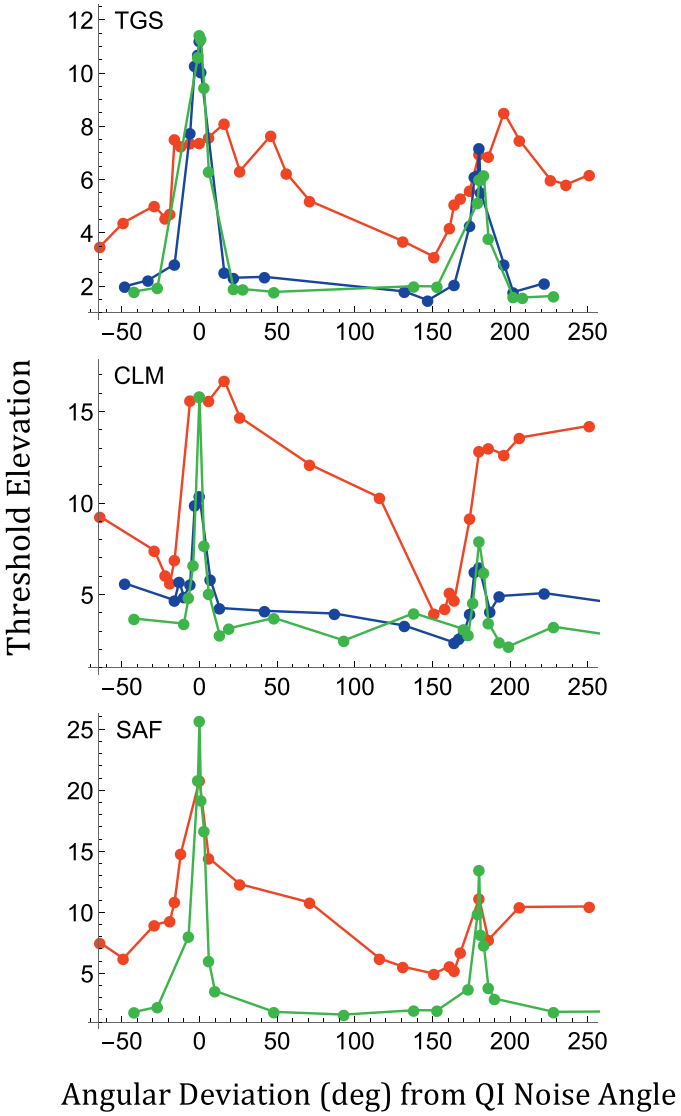

Figure 8. Threshold elevations (relative to the no-noise contour) as a function of angular deviation between the test and the noise angle in QI. Observers TGS, CLM, and SAF in the three added-noise conditions (green = 42°, blue = 48°, and red = 64°). The colors of the lines and discs are arbitrary.

intrusion of two additional mechanisms even in the no-noise case. However, across the set of four noise conditions, a total of six mechanisms are required, for all observers, as discussed next.

Our model combines the outputs of linear chromatic mechanisms by probability summation to fit detection thresholds for multiple noise conditions. The model is fit to all of the noise conditions simultaneously, with each mechanism following the test energy versus noise power relationship (Equation A1 and Appendix A). As shown later, a model with six mechanisms is able to account for data across multiple noise conditions and produce selective masking where it exists in the data (and less-selective masking where that is what the data show in the 64°/244° condition). Table 1 shows the fitted parameters, with single-letter names chosen as mnemonics based on the approximate hue of the tests at threshold. The table also provides asymptotic standard errors for the parameters. The statistical uncertainty implied by these standard errors may be visualized for one observer (TGS) in Supplementary Figure S1. The general result is that the data tightly constrain the angle and sensitivity of mechanisms responsible for detection along the flanks of the contours, but the higher thresholds at the ends of the contour make for greater uncertainty in the other mechanism angles.

Generally, the model fits the data extremely well across all of the noise conditions, accounting for a very large portion of the variance ($R^2 \geq 0.98$), but there are a few areas along some of the contours where the fit is poor (see Figures 5 through 7). For observer TGS, the model slightly overestimates the thresholds along the flanks and slightly underestimates thresholds in the corners of the 48°/228° condition. For observer CLM, the model overestimates thresholds in QI in the 64°/244° condition. There is also a slight overestimation along the greenish flank (QII) in the 42°/222° noise condition. These small discrepancies result from the constraint that the slopes of each mechanism line must be the same in across all the conditions, for each observer, because the model was fit to all of the noise conditions simultaneously (Equation A1 and Appendix A).

In some conditions for some observers, a given mechanism does not contribute to any of the thresholds. An example is shown by the blue line in Figure 4 for observers TGS and CLM. This mechanism threshold lies well outside the data, especially for TGS. Its position is determined not by the no-noise thresholds shown in Figure 4 but rather by the thresholds in the three other noise conditions because it obeys the relationship given in Equation 1. (Compare the slope of the blue line in Figure 4 with the blue lines in Figures 5, 6, and 7.) This example illustrates the fact that the model fit is applied to all of the noise conditions simultaneously and how the model constrains the fit in any one noise condition.

For two of the three observers, the mechanism vectors of R and G, and of O and B are separated by approximately 180° and are approximately equal in magnitude (i.e., they have approximate odd symmetry) and can be thought of as quasi-paired. Observer CLM is the exception. For all observers, mechanisms Y and P are not symmetric in angle or sensitivity. However, the uncertainty on the weights of the Y and P mechanisms is large because (with the partial exception of the 64°/244° noise condition) only a small segment of the mechanism threshold line is revealed in the data (Supplementary Figure S1). Importantly, fitting the

Observer	No noise	42°/222° noise	48°/228° noise	64°/244° noise
TGS	54° and 217°	44° and 225°	47° and 228°	57° and 234°
CLM	46° and 229°	43° and 223°	46° and 226°	57° and 234°
SAF	48° and 227°	40° and 222°	N/A	58° and 233°

Table 2. Peaks of the fitted contour in the no-noise, 42°/222° noise, 48°/228° noise, and 64°/244° noise conditions for observers TGS, CLM, and SAF.

model with pairs of mechanisms being required to be exactly symmetric in angle and sensitivity produced significantly worse fits (discussed below).

Table 2 gives the peaks of the detection contours in all of the noise conditions. These are not necessarily separated by 180° because the probability summation contour of asymmetric mechanisms is not symmetric. The peaks do not exactly match the noise direction, but there is clearly a selective effect.

Figure 9 summarizes the main features of the model fit with nested plots that contain all of the probability summation contours for observers TGS, CLM, and SAF plotted on the same scale. The colored points on the contours represent the noise directions, and the black dotted line indicates the main diagonal 45°/225° axis for reference. The change in the shape of the contours demonstrates that there is less selectivity as the noise angle moves away from the end of the contour (i.e., the contour is broader), a result consistent with previous studies (see Giulianini & Eskew, 1998); compare with Figure 8.

Alternative models

As noted, at least two of the six mechanisms (Y and P) are clearly asymmetrical (i.e., unpaired), with asymmetrical cone weights and different sensitivities. The other four mechanisms (R, G, B, and O) are quasi-paired: The estimated weights are not exactly equal and opposite, but the stimuli they detect appear to be approximately symmetrical along the flanks. Perhaps these quasi-paired mechanisms are actually two parallel pairs. Therefore, we refit the model, trying various symmetry constraints on the mechanisms. We constrained R and G, and B and O, to have cone weights that were equal in magnitude and opposite in sign (i.e., we made them two opponent pairs). All three model fits had $R^2 > 0.97$. However, the model fits with these symmetry and sensitivity constraints were significantly worse than the original six-mechanism model where both the mechanism's sensitivity and cone weights were free to vary, even after taking into account the reduced number of free parameters produced by the symmetry constraint. These conclusions hold whether or not the noise sensitivity parameter b was constrained to be the same for the two members of a pair. Details of these analyses are given in the Supplementary Material. Allowing slight asymmetries in the model is necessary to satisfactorily fit the data across multiple noise conditions.

A major aim of this study was to determine whether a higher order model—one with many mechanisms—was required to produce selective masking and account for the data along the detection contours. For this reason, we tested several variations on models with eight and sixteen linear mechanisms. These did not provide a significantly better fit. For the base model of Hansen and Gegenfurtner (2013) with 16 symmetric mechanisms, the fit was significantly worse than our six-mechanism model. There is no evidence in any of these analyses for there being more than six rectified mechanisms. Details are given in the Supplemental Material.

Thus, for this extensive set of data, the six-mechanism model could not be significantly improved by adding more mechanisms. Other possible models might include mechanism nonlinearities, which are particularly plausible given the high noise contrast power used in the present study. One type of nonlinearity we tried was raising the cosine terms in Equation 1 to an exponent before being squared in the power calculation—for example, $\cos^{2\gamma}(\alpha - \nu)$, with γ a free parameter—for all or some of the mechanisms. This type of nonlinearity, which has been used in several previous studies (D'Zmura & Knoblauch, 1998; Goda & Fujii, 2001; Hansen & Gegenfurtner, 2006; McKeefry, McGraw, Vakrou, & Whitaker, 2004), forces a symmetric tuning curve for the masking effect of the noise, and it failed here.

Another important and plausible nonlinear model involves adaptive changes in cone weights, resulting from the high contrast of the noises (Atick, Li, & Redlich, 1993; Zaidi & Shapiro, 1993). There is no question that some sort of adaptive model could fit our data. We have fit four linear mechanisms to each noise condition considered independently, and the fit is outstanding in all 13 cases (including observer NO, whose data are not shown). Thus, we could easily fit the entire set of data simply by slightly altering the cone contrast weights of the R and G mechanisms in each noise condition to align the long flanks of the detection contour approximately with the noise vector, and only two of the other mechanisms would be required. However, without some theoretical constraint on the

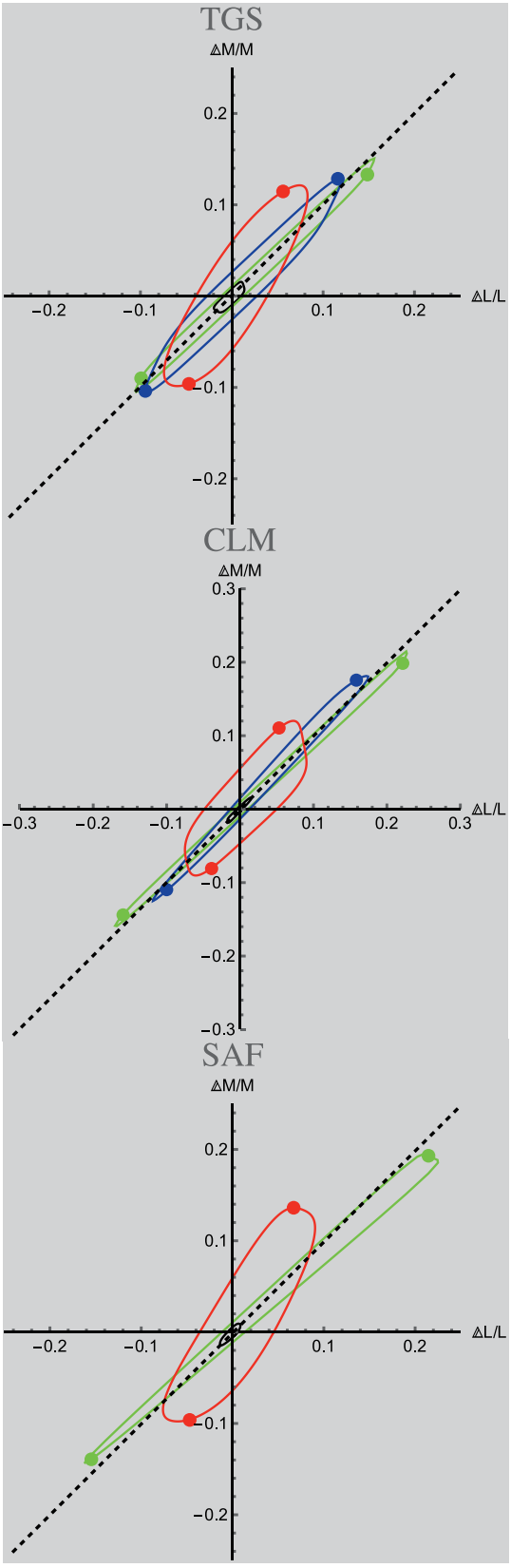

Figure 9. Predicted six-mechanism model contours in multiple noise conditions for three observers. Black = no-noise condition; green = 42°/222° noise condition; blue = 48°/228° noise condition; red = 64°/244° noise condition. The colored discs indicate the noise direction, and the black dotted line indicates the main diagonal (45°/225° axis) for reference. The contour tilts toward the noise direction, and, consistent with previous results (Eskew, Newton, & Giulianini, 2001; Giulianini & Eskew, 1998), there is less selectivity as the noise is moved away from the ends of the contour.

adjustment of the weights across noise conditions, this four-mechanism adaptive model would be nearly impossible to disprove (Eskew, 2009).

In addition, informal observations by our observers suggest that the hues of the thresholds fall into six—not four—categories. Therefore, as attractive an idea as the adaptive mechanism model is, it is unlikely that such a model could account for the subjective experience resulting from these mechanisms (i.e., the hues produced by the mechanisms). A study of the color appearance of tests detected by these mechanisms is currently in progress.

General discussion and conclusions

The asymmetries in thresholds we observed in this study, taken together with related asymmetries observed in other studies (e.g., Krauskopf et al., 1982; Krauskopf & Zaidi, 1986; Vingrys & Mahon, 1998; Wang et al., 2014), imply that experiments using bipolar stimuli, such as Gabor patches or gratings, are likely to miss important features of the data because detection contours measured with such stimuli are required to be symmetric. It seems likely that bipolar stimuli will generate detection contours that are the inner envelope produced by the set of mechanisms (i.e., the most sensitive mechanisms will dominate) and perhaps therefore miss theoretically important features of the data.

We replicated the main result of Hansen and Gegenfurtner (2013): The effect of the noise could be selective. The maximum threshold elevation was at or near the noise direction in the 42°/222° and 48°/228° conditions (Figure 8). Masking at 64°/244° was less selective, suggesting a transition to nonselective masking as the noise is moved away from the ends of the detection contour. This is consistent with previous results showing nonselective masking when noise was placed in QII/QIV of this plane in color space—that is, noises at 90°/270° (M-cone noise), 120°/300°, 135°/315°, and 0°/180° (L-cone noise; Eskew et al., 2001; Giulianini & Eskew, 1998)—although those noises were of lower power than those used in the present study and in Hansen and Gegenfurtner (2013).

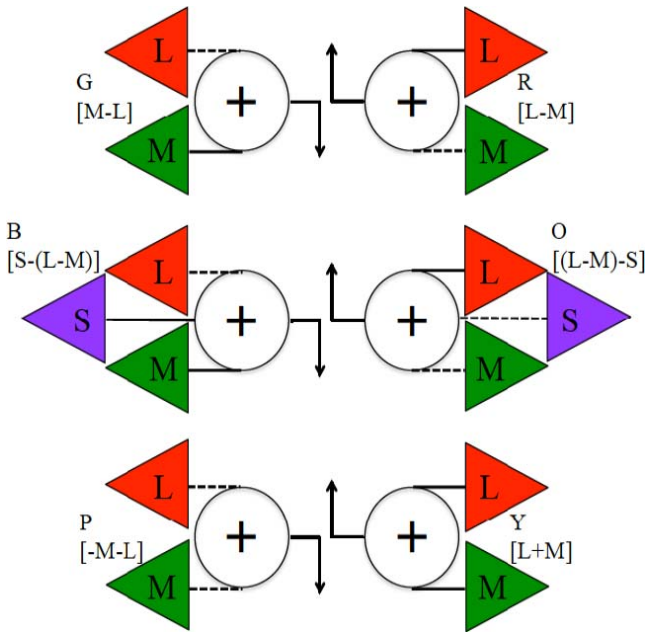

Figure 10. Six-mechanism model. The dashed lines indicate sign inversion (subtraction). Each mechanism is half-wave rectified. Four of these mechanisms (R and G, and B and O) are quasipaired, having nearly equal and opposite L- and M-cone weights. Two mechanisms (Y and P) have additive L- and M-cone inputs and are asymmetric (unpaired). The S-cone input to B and O is by analogy to the cardinal model (Figure 1); it was not studied in the present experiments.

Hansen and Gegenfurtner (2013) noted this difference between their study and our earlier experiments (Giulianini & Eskew, 1998): Their noise had a peak cone contrast vector length of 0.4, whereas Giulianini and Eskew used peaks averaging about 0.04 in most conditions. In the present study, our peak cone contrast vector lengths (after accounting for half toning) are about 0.50, 0.41, and 0.27 for the 42°/222°, 48°/228°, and 64°/244° noise conditions, respectively. However, the noise used by Hansen and Gegenfurtner (2013) was drawn from a uniform probability distribution, whereas our noise (like that of Giulianini & Eskew, 1998) was binary, which produces greater power (Gegenfurtner & Kiper, 1992). For the same peak values, the variance (and hence the contrast power) of a uniform distribution is threefold lower than that of the Bernoulli (binary) distribution with the same maximum values because many of the samples from the uniform distribution lie close to zero. Thus, the Hansen and Gegenfurtner (2013) peak noise contrast of 0.4 has power that is equivalent to a binary noise with peak contrast of 0.23, comparable to our weakest noise. Therefore, the less-selective effect of the 64°/244° noise in our study, which our model predicts, is not merely because the noise does not have enough power.

We show that a model can produce this selective masking with only six linear mechanisms—the same number as the cardinal mechanism model. Adding more than six mechanisms never significantly improved the fit. The main point of this study is that selective masking is not evidence for large numbers of mechanisms, which differs from the conclusion of Hansen and Gegenfurtner (2013). In fact, our model predicts selective masking for noises across a range of angles near 45°/225° in cone contrast space (calculations not shown) and the much wider corresponding range of angles in threshold-scaled MBDKL space. The model also predicts much less selectivity for noises away from the ends of the detection contour (e.g., Figure 7) with the same six mechanisms. This conclusion does not depend on the use of the unipolar test stimulus. We have shown the same selective masking with Gabor patch tests, and a six-mechanism (necessarily symmetric) model could account for those selective masking results as well (Eskew & Shepard, 2013; Shepard, Swanson, & Eskew, 2013).

The model of Table 1 is depicted in Figure 10. S-cone input is shown to two of the mechanisms to be as similar as possible to the cardinal model of Figure 1. The assignment of this S-cone input to these particular mechanisms is speculative here because we did not modulate S-cones in the present experiment. However, it is important to keep in mind that any linear postreceptoral mechanism(s) receiving S-cone input will be active in the (L,M) plane (the sole exception being a mechanism that gets *only* S-cone input, for which there is no evidence). Because some of the mechanisms of Figure 10 must get S-cone input, we have depicted it in the figure for completeness. Although the cardinal model (Figure 1) has the S-cone input opposed by a sum of L and M, substantial prior evidence indicates that S-cone detection mechanisms have long-wavelength inputs of opposite sign, as shown here (De Valois & De Valois, 1993; McLellan & Eskew, 2000; Wang et al., 2014; Wisowaty, 1983).

Although our model has six mechanisms like the elaborated cardinal model of Figure 1, our model differs in one important respect: Four of our six detection mechanisms have opposed L- and M-cone inputs rather than only two. This—not its asymmetry (see Supplementary Material)—is the essential feature of our model that allows it to account for selective masking when noise is placed near the ends of the detection contour in the (L,M) plane. Noises that are nearly parallel to the long flanking detection contours can cause different mechanisms to become most sensitive and thus determine threshold, tilting the overall detection contour. Further study of the properties of these mechanisms is ongoing.

It is difficult to relate any psychophysical threshold model to the activity of visual cortical neurons, in part

because behavioral thresholds are likely dominated by the most sensitive subset of cells. Nonetheless, there are several possible points of comparison between our model and cortical neurons—at least those with foveal or near-foveal receptive fields. First, the mechanisms in our model are, at least to a good approximation, linear combinations of cone signals. Some cortical neurons respond to linear cone combinations, especially in V1, but others are nonlinear and thus more narrowly or more broadly tuned (De Valois, Cottaris, Elfar, Mahon, & Wilson, 2000; Horwitz & Hass, 2012; Lennie, Krauskopf, & Sclar, 1990). It is not generally clear how sensitive the linear cells are compared with the nonlinear ones. Second, there are only six mechanisms in our model, which might suggest that the especially sensitive cells would fall into six clusters in terms of their cone weights. Many physiological studies report cells with a large variety of chromatic tunings (De Valois et al., 2000; Horwitz & Hass, 2012; Komatsu, 1998), but again it is not clear that these are highly sensitive or even that they all actually have to do with color vision (e.g., Horwitz & Hass, 2012). The fact that they respond to chromatic stimuli might only be a result of irrelevant variation in cone connectivity (Conway, 2009). Third, based on our model, most of the sensitive cells should have opposed L- and M-cone inputs; L–M opponency is common in many cortical cells, but it is not clear that it predominates (e.g., Horwitz & Hass, 2012). Fourth—and most optimistically—the cells might have cone contrast weights similar to those in Table 1. Of course, it is important to keep in mind that, even among cortical cells that actually serve color vision, there are likely to be neurons that do not satisfy the definition of psychophysical color mechanisms: univariant labeled lines with fixed relative spectral tuning (e.g., tuning may change with contrast; Horwitz & Hass, 2012; Namima, Yasuda, Banno, Okazawa, & Komatsu, 2014; Solomon & Lennie, 2005; for discussion see Eskew, 2009).

Keywords: color vision, chromatic detection, color mechanisms

Acknowledgments

This research was supported by NSF Grant BCS-1353338. The authors are grateful for comments on the article by Karl Gegenfurtner and Thorsten Hansen and for the hard observing work of Safiya Lahlaf and Nicole Ochandarena.

Commercial relationships: none.
Corresponding author: Timothy G. Shepard.
Email: shepard.ti@husky.neu.edu.
Address: Department of Psychology, Northeastern University, Boston, MA, USA.

References

Atick, J. J., Li, Z., & Redlich, A. N. (1993). What does post-adaptation color appearance reveal about cortical color representation? *Vision Research, 33,* 123–129, doi:10.1016/0042-6989(93)90065-5.

Boynton, R. M. (1979). *Human color vision*. New York, NY: Holt, Rinehart, & Winston.

Burgess, A., Wagner, R., Jennings, R., & Barlow, H. (1981). Efficiency of human visual signal discrimination. *Science, 214,* 93–94, doi:10.1126/science.7280685.

Chaparro, A., Stromeyer, C. F., III, Huang, E. P., Kronauer, R. E., & Eskew, R. T., Jr. (1993). Colour is what the eye sees best. *Nature, 361,* 348–350, doi:10.1038/361348a0.

Cole, G. R., Hine, T., & McIlhagga, W. (1993). Detection mechanisms in L-, M-, and S-cone contrast space. *Journal of the Optical Society of America A, 10,* 38–51, doi:10.1364/JOSAA.10.000038.

Cole, G. R., Stromeyer, C. F., III, & Kronauer, R. E. (1990). Visual interactions with luminance and chromatic stimuli. *Journal of the Optical Society of America, 7,* 128–140, doi:10.1364/JOSAA.7.000128.

Conway, B. R. (2009). Color vision, cones, and color-coding in the cortex. *Neuroscientist, 15,* 274–290, doi:10.1177/1073858408331369.

De Valois, R. L., Cottaris, N. P., Elfar, S. D., Mahon, L. E., & Wilson, J. A. (2000). Some transformations of color information from lateral geniculate nucleus to striate cortex. *Proceedings of the National Academy of Sciences, USA, 97,* 4997–5002, doi:10.1073/pnas.97.9.4997.

De Valois, R. L., & De Valois, K. (1993). A multi-stage color model. *Vision Research, 33,* 1053–1065.

D'Zmura, M., & Knoblauch, K. (1998). Spectral bandwidths for the detection of color. *Vision Research, 38,* 3117–3128, doi:10.1016/S0042-6989(97)00381-7.

Eskew, R. T., Jr. (2009). Higher order color mechanisms: A critical review. *Vision Research, 49,* 2686–2704, doi:10.1016/j.visres.2009.07.005.

Eskew, R. T., Jr., Newton, J., & Giulianini, F. (2001). Chromatic detection and discrimination analyzed by a Bayesian classifier. *Vision Research, 41,* 893–909, doi:10.1016/S0042-6989(00)00298-4.

Eskew, R. T., Jr., McLellan, J. S., & Giulianini, F. (1999). Chromatic detection and discrimination. In K. R. Gegenfurtner & L. T. Sharpe (Eds.), *Color vision: From genes to perception* (pp. 345–368). Cambridge, United Kingdom: Cambridge University Press.

Eskew, R. T., Jr., & Shepard, T. G. (2013). Highly-selective chromatic masking does not require large numbers of color mechanisms. *Journal of Vision, 13*(9): 296, doi:10.1167/13.9.296. [Abstract]

Farnsworth, D. (1943). The Farnsworth-Munsell 100-hue and dichotomous tests for color vision. *Journal of the Optical Society of America, 33,* 568–578, doi:10.1364/JOSA.33.000568.

Gegenfurtner, K. R., & Kiper, D. C. (1992). Contrast detection in luminance and chromatic noise. *Journal of the Optical Society of America A, 9,* 1880–1888, doi:10.1364/JOSAA.9.001880.

Giulianini, F., & Eskew, R. T., Jr. (1998). Chromatic masking in the (delta L/L, delta M/M) plane of cone-contrast space reveals only two detection mechanisms. *Vision Research, 38,* 3913–3926, doi:10.1016/S0042-6989(98)00068-6.

Giulianini, F., & Eskew, R. T., Jr. (2007). Theory of chromatic noise masking applied to testing linearity of S-cone detection mechanisms. *Journal of the Optical Society of America A, 24,* 2604–2621, doi:10.1364/JOSAA.24.002604.

Goda, N., & Fujii, M. (2001). Sensitivity to modulation of color distribution in multicolored textures. *Vision Research, 41,* 2475–2485, doi:10.1016/S0042-6989(01)00136-5.

Hansen, T., & Gegenfurtner, K. R. (2006). Higher level chromatic mechanisms for image segmentation. *Journal of Vision, 6*(3):5, 239–259, doi:10.1167/6.3.5. [PubMed] [Article]

Hansen, T., & Gegenfurtner, K. R. (2013). Higher order color mechanisms: Evidence from noise-masking experiments in cone contrast space. *Journal of Vision, 13*(1):26, 1–21, doi:10.1167/13.1.26. [PubMed] [Article]

Horwitz, G. D., & Hass, C. A. (2012). Nonlinear analysis of macaque V1 color tuning reveals cardinal directions for cortical color processing. *Nature Neuroscience, 15,* 913–919, doi:10.1038/nn.3105.

Komatsu, H. (1998). Mechanisms of central color vision. *Current Opinion in Neurobiology, 8,* 503–508, doi:10.1016/S0959-4388(98)80038-X.

Krauskopf, J. (1999). Higher order color mechanisms. In K. R. Gegenfurtner & L. T. Sharpe (Eds.), *Color vision: From genes to perception* (pp. 303–316). Cambridge, United Kingdom: Cambridge University Press.

Krauskopf, J., Williams, D. R., & Heeley, D. W. (1982). Cardinal directions of color space. *Vision Research, 22,* 1123–1131, doi:10.1016/0042-6989(82)90077-3.

Krauskopf, J., Williams, D. R., Mandler, M. B., & Brown, A. M. (1986). Higher order color mechanisms. *Vision Research, 26*(1), 23–32, doi:10.1016/0042-6989(86)90068-4.

Krauskopf, J., & Zaidi, Q. (1986). Induced desensitization. *Vision Research, 26,* 759–762, doi:10.1016/0042-6989(86)90090-8.

Legge, G. E., Kersten, D., & Burgess, A. E. (1987). Contrast discrimination in noise. *Journal of the Optical Society of America A, 4,* 391–404, doi:10.1364/JOSAA.4.000391.

Lennie, P., & D'Zmura, M. (1988). Mechanisms of color vision. *Critical Reviews in Neurobiology, 3,* 333–400.

Lennie, P., Krauskopf, J., & Sclar, G. (1990). Chromatic mechanisms in striate cortex of macaque. *Journal of Neuroscience, 10,* 649–669.

McKeefry, D. J., McGraw, P. V., Vakrou, C., & Whitaker, D. (2004). Chromatic adaptation, perceived location, and color tuning properties. *Visual Neuroscience, 21,* 275–282, doi:10.1017/S0952523804213426.

McLellan, J. S., & Eskew, R. T., Jr. (2000). ON and OFF S-cone pathways have different long-wave cone inputs. *Vision Research, 40,* 2449–2465, doi:10.1016/S0042-6989(00)00107-3.

Namima, T., Yasuda, M., Banno, T., Okazawa, G., & Komatsu, H. (2014). Effects of luminance contrast on the color selectivity of neurons in the macaque area V4 and inferior temporal cortex. *Journal of Neuroscience, 34,* 14934–14947, doi:10.1523/jneurosci.2289-14.2014.

Newton, J. R., & Eskew, R. T., Jr. (2003). Chromatic detection and discrimination in the periphery: A postreceptoral loss of color sensitivity. *Visual Neuroscience, 20,* 511–521, doi:10.1017/S0952523803205058.

Pelli, D. G. (1981). *Effects of visual noise*. Cambridge, United Kingdom: Cambridge University Press.

Sankeralli, M. J., & Mullen, K. T. (1996). Estimation of the L-, M-, and S-cone weights of the postreceptoral detection mechanisms. *Journal of the Optical Society of America A, 13,* 906–915, doi:10.1364/JOSAA.13.000906.

Sankeralli, M. J., & Mullen, K. T. (1997). Postreceptoral chromatic detection mechanisms revealed by

noise masking in three-dimensional cone contrast space. *Journal of the Optical Society of America A, 14,* 2633–2646, doi:10.1364/JOSAA.14.002633.

Sankeralli, M. J., & Mullen, K. T. (2001). Bipolar or rectified chromatic detection mechanisms? *Visual Neuroscience, 18,* 127–135, doi:10.1017/S0952523801181125.

Shepard, T. G., Swanson, E. A., & Eskew, R. T., Jr. (2013). Color mechanisms revealed by measuring detection and discrimination together. *Journal of Vision, 13*(9): 1013, doi:10.1167/13.9.1013. [Abstract]

Solomon, S. G., & Lennie, P. (2005). Chromatic gain controls in visual cortical neurons. *Journal of Neuroscience, 25,* 4779–4792, doi:10.1523/JNEUROSCI.5316-04.2005.

Vingrys, A. J., & Mahon, L. E. (1998). Color and luminance detection and discrimination asymmetries and interactions. *Vision Research, 38,* 1085–1095, doi:10.1016/S0042-6989(97)00250-2.

Wang, Q., Richters, D. P., & Eskew, R. T., Jr. (2014). Noise masking of S-cone increments and decrements. *Journal of Vision, 14*(13):8, 1–17, doi:10.1167/14.13.8. [PubMed] [Article]

Wisowaty, J. J. (1983). An action spectrum for the production of transient tritanopia. *Vision Research, 23,* 769–774, doi:10.1016/0042-6989(83)90199-2.

Zaidi, Q., & Shapiro, A. G. (1993). Adaptive orthogonalization of opponent-color signals. *Biological Cybernetics, 69,* 415–428, doi:10.1007/BF01185413.

Appendix A

The threshold contrast energy of an achromatic (Burgess, Wagner, Jennings, & Barlow, 1981; Pelli, 1981) or chromatic (Gegenfurtner & Kiper, 1992; Giulianini & Eskew, 1998) test stimulus may be described by a linear function of the contrast power of the noise. We refer to this relationship as an empirical energy versus noise function, expressed as

$$E = N_0 + N, \tag{A1}$$

where E represents the test contrast energy (proportional to squared contrast), N is the applied noise contrast power (also proportional to squared contrast), and N_0 is a constant representing the level of intrinsic noise in the detection mechanism. For a rectified but otherwise linear chromatic detection mechanism, Equation A1 may be written as

$$Q_t \lfloor \mathbf{f} \cdot \mathbf{t} \rfloor^2 = N_0 + bQ_n \lfloor \mathbf{f} \cdot \mathbf{n} \rfloor^2 \tag{A2}$$

(compare equation 9 of Wang et al., 2014). In Equation A2, $\mathbf{f}$ is the vector of cone contrast weights of the mechanism, (W_L, W_M). The vector $\mathbf{t}$ represents the cone contrasts ($\Delta L/L$, $\Delta M/M$) of the test, and $\mathbf{n}$ is the corresponding vector representing the noise. The half brackets ($\lfloor\ \rfloor$) represent half-wave rectification (i.e., values less than zero are set to zero).

Q_n is the constant of proportionality between the noise contrast squared and the noise power. Its value was taken to be the unit contrast noise power at DC, which is 1.07×10^{-3} deg·s, after accounting for half toning. This value was calculated in Wang et al. (2014) for radially symmetric noise. The value here is the same considering the vertical dimension of the pattern. The analogous constant for the contrast energy of the blob test, again considering only the vertical dimension, is

$$\begin{aligned} Q_t &= \int_0^{+\infty} \int_{-\infty}^{+\infty} \left(h(t) w(y) e^{-y/2} \right)^2 dy\, dt \\ &= 0.111 \frac{\sqrt{\pi}}{2} \text{ deg} \cdot \text{sec}, \end{aligned} \tag{A3}$$

in which $h(t)$ gives the time course of the test presentation (Figure 2b) and $w(y)$ is the half-toning function (which sets alternate 2-pixel lines to zero contrast). Explicitly including Q_t and Q_n in the model factors these stimulus-specific constants out of the mechanism vector and, in principle, makes the cone contrast weights independent of the spatiotemporal characteristics of the test and noise. Comparison with previously published cone contrast mechanism vector lengths from studies that did not explicitly take the Qs into account (e.g., the summary in Eskew et al., 1999) requires multiplying the vector lengths in Table 1 by $\sqrt{Q_t}$.

Without loss of generality we can let $N_0 = 1$, effectively scaling in terms of the intrinsic noise. It is convenient to express the relationship of Equation A2 in polar coordinates:

$$Q_t |\mathbf{f}|^2 |\mathbf{t}|^2 \lfloor \cos(\alpha - \tau) \rfloor^2 = 1 + bQ_n |\mathbf{f}|^2 |\mathbf{n}|^2 \lfloor \cos(\alpha - v) \rfloor^2,$$

where α, τ, and v are the angles of the mechanism, test, and noise vectors, respectively, in the (L,M) plane. The vector length of the test at threshold is then

$$|\mathbf{t}| = \sqrt{\frac{1}{Q_t |\mathbf{f}|^2 \lfloor \cos(\alpha - \tau) \rfloor^2} + b \frac{Q_n}{Q_t} \frac{|\mathbf{n}|^2 \lfloor \cos(\alpha - v) \rfloor^2}{\lfloor \cos(\alpha - \tau) \rfloor^2}}. \tag{A4}$$

The first term in the radical represents the mechanism thresholds in the absence of noise and, at a given test angle, is inversely proportional to the mechanism vector length, $|\mathbf{f}|$. The second term in the radical represents the effect of the noise (of contrast $|\mathbf{n}|$). Because the mechanism sensitivity $|\mathbf{f}|$ affects the response to the noise and the test equally, the

mechanism vector length does not appear in the second term, which is to say that the *relative* degree of elevation by the noise does not depend on the sensitivity of the mechanism. Equation A4 was applied to each mechanism, simultaneously across all the noise conditions, to estimate values of the cone weights (W_L, W_M; determining $|\mathbf{f}|$ and α) and b, with the responses of the mechanisms combined by probability summation (Minkowski exponent of 4.0; Eskew et al., 1999).

Because thresholds in the no-noise condition are lower and thus more similar to one another, their variance is less than in the noise conditions (especially the 42°/222° and 48°/228° noise conditions). Without compensating for this difference in some way, the no-noise condition data would contribute much less to the fitting of the model. Therefore, in fitting the model for each observer, the data from each noise condition were weighted inversely to the variance of the thresholds in that condition.

It is worth comparing our modeling approach to the approach of Hansen and Gegenfurtner (2006). These authors did not fit their model, which contained a total of 4,096 mechanisms after the 16 pairs of base cone weights were randomly perturbed, to their data. Instead, a Monte Carlo procedure was used to find tests $\mathbf{t}$ that would produce a threshold response in the presence of chromatic noise, with the vector of cone weights $\mathbf{f}$ fixed for each hypothetical mechanism. Because we were fitting measured thresholds, we varied the mechanism parameters instead of varying simulated tests. Stated simply, for a single mechanism and noise condition, we found the vector of cone weights $\mathbf{f}$ that satisfied $\mathbf{f}\cdot\mathbf{t} = 1$, with $\mathbf{t}$ determined by experiment, whereas Hansen and Gegenfurtner (2006) found values of $\mathbf{t}$ satisfying the same relationship, with $\mathbf{f}$ determined by assumption.